Abrupt symmetry-preserving transition from the chimera state

M. Manoranjani
Department of Physics, Centre for Nonlinear Science and Engineering, School of Electrical and Electronics Engineering, SASTRA Deemed University, Thanjavur 613 401, India

D. V. Senthilkumar*
School of Physics, Indian Institute of Science Education and Research, Thiruvananthapuram-695016, India

V. K. Chandrasekar†
Department of Physics,Centre for Nonlinear Science and Engineering, School of Electrical and Electronics Engineering, SASTRA Deemed University, Thanjavur 613 401, India

(Received 29 January 2023; accepted 9 March 2023; published 24 March 2023)

We consider two populations of the globally coupled Sakaguchi-Kuramoto model with the same intra- and interpopulations coupling strengths. The oscillators constituting the intrapopulation are identical whereas the interpopulations are nonidentical with a frequency mismatch. The asymmetry parameters ensure the permutation symmetry among the oscillators constituting the intrapopulation and a reflection symmetry among the oscillators constituting the interpopulation. We show that the chimera state manifests by spontaneously breaking the reflection symmetry and also exists in almost in the entire explored range of the asymmetry parameter without restricting to the near $\pi/2$ values of it. The saddle-node bifurcation mediates the abrupt transition from the symmetry breaking chimera state to the symmetry-preserving synchronized oscillatory state in the reverse trace, whereas the homoclinic bifurcation mediates the transition from the synchronized oscillatory state to synchronized steady state in the forward trace. We deduce the governing equations of motion for the macroscopic order parameters employing the finite-dimensional reduction by Watanabe and Strogatz. The analytical saddle-node and homoclinic bifurcation conditions agree well with the simulations results and the bifurcation curves.

DOI: 10.1103/PhysRevE.107.034212

I. INTRODUCTION

Spontaneous segregation of symmetrically coupled identical oscillators into synchronized and desynchronized subpopulations as observed by Kuramoto and Battogotokh [1] was a surprising phenomenon in early 2000, which was unprecedented in the nonlinear dynamics literature. The momentum in investigating the partially synchronized state has been increased immediately after such a self-organizing phenomenon has been coined as the "chimera state" by Abrams and Strogatz [2]. Initially, the chimera state has been reported in populations of nonlocally coupled oscillators, such as the Ginzburg-Landau systems, Rössler oscillators, and logistic maps [3–6]. Later, the existence of chimera states has also been reported extensively in nonlocally coupled identical phase oscillators [1,2,7–9]. Even though promising results have been published employing nonlocally coupled nonlinear oscillators both experimentally [10–13] and theoretically [1,5,14,15], the necessity of the nonlocal nature of the coupling posed a serious restriction to generalize the studies on chimera states to other prominent coupling configurations, which, in turn, has limited its applications. Later studies have extended the notion of the chimera state to even the globally coupled one and two populations of nonlinear oscillators [16–22], including complex and multilayer networks [23–28],

The phenomenon of spontaneous symmetry breaking is ubiquitous in nature, a source for a plethora of nontrivial self-organizing patterns and intriguing dynamical states. Complex pattern formation in the neuronal networks is often found to be mediated by the spontaneous symmetry breaking phenomenon [29]. The transition from the amplitude death state to the oscillation death state via the Turing bifurcation was shown to be mediated by the spontaneous symmetry breaking phenomenon [30,31]. In general, the emergence of heterogeneous (asymmetric) dynamical states from symmetrically coupled oscillator networks are usually due to the spontaneous symmetry breaking phenomenon [32–34]. The chimera state is indeed such a spontaneous symmetry breaking state that emerges by breaking the prevailing symmetry of the dynamical states. The onset of the chimera state spontaneous breaks the spatial rotational symmetry of an array of nonlocally coupled oscillators. The permutation symmetry prevailing among the globally coupled oscillators is broken by the manifestation of the chimera state. The symmetries within and among two or more populations of globally and nonlocally coupled nonlinear oscillators [33,34] are broken due to the birth of the chimera state. For instance, it has been recently reported that the onset of the local chimera is accompanied by the spontaneous symmetry breaking of the globally coupled subpopulation with a smaller frequency whereas retaining the

*Corresponding author: skumarusnld@gmail.com
†chandru25nld@gmail.com

symmetry of the synchronized subpopulation with a larger frequency [34].

In this paper, we consider two populations of the globally coupled Sakaguchi-Kuramoto model with the same coupling strength for both intrapopulation and interpopulation interactions. The oscillators constituting the intrapopulations are identical with the same frequency but with a frequency mismatch between the interpopulation. There is a permutation symmetry within the intrapopulations and a reflection symmetry between the interpopulation unlike the case of Abrams *et al.* [16] where there exists the permutation symmetry in both intrapopulations and interpopulation both due to the nature of the employed asymmetry parameters. Note that Abrams *et al.* [16] considered the intrapopulation coupling strength greater than the interpopulation coupling strength and identified chimera states for large values of the asymmetry parameter. We unravel the existence of the chimera state in a rather large range of the asymmetry parameter extending even to near zero values of the latter and not just restricting only to near $\pi/2$ values of the asymmetry parameter as reported in the literature [16–20,23,24,26,27].

The chimera state in the current setup emerges by spontaneously breaking the reflection symmetry among the interpopulation unlike the existing literature on two or more populations where the chimera states usually emerge by breaking the permutation symmetry among the interpopulation [29]. It is interesting to note that such a spontaneous breaking of the mirror (reflection) symmetry is observed in the chiral inorganic nanocrystal during the chiral amplification below a critical temperature [35]. The two-parameter phase diagrams reveal the coexistence of two types of symmetry preserving synchronized state with the symmetry breaking chimera state. The synchronized state can be an oscillatory state or a stable steady state depending on the parameters. Furthermore, there is an abrupt transition from the symmetry breaking state to the symmetry-preserving state during the backward trace, whereas the two populations remain synchronized in the forward trace. We also deduce the governing equations of motion for the macroscopic order parameters employing the finite-dimensional reduction by Watanabe and Strogatz [36]. The deduced analytical stability curves, from the evolution equations of motion for the macroscopic order parameters, corresponding to the saddle-node and homoclinic (Hc) bifurcations are found to exactly match with the simulations results and the bifurcation curves obtained using the software package XPPAUT [37].

The paper is organized as follows. We introduce the Sakaguchi-Kuramoto model in Sec. II. We deduce the evolution equations corresponding to the macroscopic order parameters using the Cestnik and Pikovsky ansatz in Sec. III. In Sec. IV, we illustrate the phase diagrams and discuss the dynamical transitions across various bifurcation scenarios demarcating the dynamical states in the phase diagrams. Finally, we will provide a summary and conclusions in Sec. V.

II. MODEL

We consider two populations of globally coupled Sakaguchi-Kuramoto model, whose evolution equations are governed by the set of N coupled first order nonlinear ordinary differential equations represented as

$$\dot{\xi}_i^\sigma = \omega^\sigma + \sum_{\sigma'=1}^{2} \frac{K^{\sigma\sigma'}}{N} \sum_{j=1}^{N^{\sigma'}} \sin(\xi_j^{\sigma'} - \xi_i^\sigma + \alpha^{\sigma\sigma'}), \quad (1)$$

where $\sigma = 1, 2$ represents the first and the second populations. ξ_i^σ is the phase of the ith oscillator in the population σ. ω^σ is the natural frequency of the oscillators in the population σ. Note that all oscillators in the intrapopulation are chosen to be identical, whereas there is a frequency mismatch between the interpopulation. The coupling strengths between the populations are given by $K^{\sigma\sigma'}$. We choose $K^{11} = K^{22} = K^{12} = K^{21} = K$, so the intrapopulation coupling strength is equal to the interpopulation coupling strength. The asymmetric parameters in the intrapopulation and interpopulation couplings have a σ' dependency. If $\sigma' = 1$, then, $\alpha^{\sigma\sigma'} = -\alpha$ and $\sigma' = 2$, then, $\alpha^{\sigma\sigma'} = +\alpha$ irrespective of σ resulting in the asymmetry parameters $\alpha^{11} = \alpha^{21} = -\alpha$ and $\alpha^{12} = \alpha^{22} = +\alpha$. It is to be noted that the Sakaguchi-Kuramoto model is symmetric about its mean frequency $\omega_0 = \frac{\omega^1+\omega^2}{2}$. Under the rotational transformation $\xi_j^\sigma = \theta_j^\sigma + \omega_0 t$, Eq. (1) in the rotational coordinates becomes

$$\dot{\theta}_i^\sigma = \gamma^\sigma + \sum_{\sigma'=1}^{2} \frac{K^{\sigma\sigma'}}{N} \sum_{j=1}^{N^{\sigma'}} \sin(\theta_j^{\sigma'} - \theta_i^\sigma + \alpha^{\sigma\sigma'}), \quad (2)$$

where $\gamma^1 = -\gamma^2 = \omega$ and $\omega = \frac{\omega^1-\omega^2}{2}$. Due to this transformation, the symmetry $\xi_j^1 = \omega_0 t + \theta_j$ and $\xi_j^2 = \omega_0 t - \theta_j$ in the original system has transformed as $\theta_j^1 = -\theta_j^2 = \theta_j$ in the rotational coordinate system, reflecting a reflection symmetry in the rotating frame of reference.

III. DIMENSIONAL REDUCTION

In this section, we adopt the finite-dimensional reduction by Watanabe and Strogatz [36] to reduced the dynamics of the system (2) from N dimensions to six dimensions by means of the Pikovsky and Rosenblum [38] transformation and Hong and Strogatz [39]. Following which, Eq. (2) can be rewritten as

$$\dot{\theta}_i^\sigma = \omega^\sigma + \mathrm{Im}(F^\sigma e^{-i\theta_i^\sigma}), \quad (3a)$$

$$F^\sigma = \sum_{\sigma'=1}^{2} K^{\sigma\sigma'} (r^{\sigma'} e^{i\phi^{\sigma'}} e^{i\alpha^{\sigma\sigma'}}), \quad (3b)$$

where F^σ is the effective force acting on the oscillators of the population σ and $r(t)e^{i\phi(t)} = 1/N \sum_{j=1}^{N} e^{i\theta_j}$. Note that all the oscillators in the given population are governed by the same equation of motion, although, generally, they have different initial conditions. Thus, the ansatz reduces the dynamics of the each population to the evolution equation in three variables $\rho^\sigma(t)$, $\Theta^\sigma(t)$, and $\Psi^\sigma(t)$, via the transformation,

$$\tan\left[\frac{\theta_i^\sigma - \Theta^\sigma}{2}\right] = \frac{1-\rho^\sigma}{1+\rho^\sigma} \tan\left[\frac{\psi_i^\sigma - \Psi^\sigma}{2}\right], \quad (4)$$

with N constants ψ_i^σ, which are directly determined from the initial state $\theta_i^\sigma(0)$. Using Eq. (3), the evolution equations for ρ, Ψ, and Θ can be written as

$$\dot{\rho}^\sigma = \frac{1-\rho^{\sigma 2}}{2}\mathrm{Re}(F^\sigma e^{-i\Theta^\sigma}), \tag{5a}$$

$$\dot{\Psi}^\sigma = \frac{1-\rho^{\sigma 2}}{2\rho}\mathrm{Im}(F^\sigma e^{-i\Theta^\sigma}), \tag{5b}$$

$$\dot{\Theta}^\sigma = \omega^\sigma + \frac{1+\rho^2}{2\rho}\mathrm{Im}(F^\sigma e^{-i\Theta^\sigma}). \tag{5c}$$

In order to endow the new variables with physical meaning, let us consider how they characterize the distribution of the phases of the given population. Generally, oscillators are distributed in a certain fashion during their evolution, and the amplitude ρ characterizes the width of the distribution, which is roughly proportional to the mean-field amplitude $r(t)$. $\rho = r = 0$ characterizes the uniform distribution of the oscillators, which corresponds to the asynchrony of the population, whereas $\rho = r = 1$ characterizes the completely synchronized state of the considered population if the distribution shrinks to the δ function. The intermediate values of $\rho = r$ between 0 and 1 characterize the partially synchronized states. The phase variable Θ is related to the phase of the mean-field $\Theta(=\phi)$, whereas the other phase variable Ψ describes the drift of the individual oscillators with respect to the mean field.

The set of Eqs. (5) is a straightforward generalization of the equations [4] to the population σ. For a further analysis, and, in particular, for the consideration in the thermodynamic limit, it is convenient to introduce two new variables, namely, a phase shift variable $\delta^\sigma = \Theta^\sigma - \Psi^\sigma$, and a complex mean-field variable $z^\sigma = \rho^\sigma e^{i\Theta^\sigma}$. Now, Eqs. (5a)–(5c) can be rewritten in terms of the complex mean-field and the phase shift variables as

$$\dot{z}^\sigma = i\omega^\sigma z^\sigma + \frac{1}{2}F^\sigma - \frac{z^{\sigma 2}}{2}F^{\star\sigma}, \tag{6a}$$

$$\dot{\delta}^\sigma = \omega^\sigma + \mathrm{Im}(z^{\star\sigma}F^\sigma). \tag{6b}$$

Remarkably, Eq. (6a) coincides with the low-dimensional evolution equations of the Ott-Antonsen theory [40,41] but without the governing equation for the phase shift variable. The above system of low-dimensional coupled nonlinear ordinary differential equations are the evolution equations for the macroscopic order parameters of the model (2), which describes the latter dynamics faithfully. Note that the governing equation for the phase shift variables are decoupled from the evolution equation for the complex mean-field variables $z^\sigma = r^\sigma e^{i\phi^\sigma} = X^\sigma + iY^\sigma$ and, hence, the dynamics of (2) can be effectively described by the evolution equations in the four variables r^σ and ϕ^σ, where $\sigma = 1, 2$ [39]. In the following, we represent σ corresponding to the first and second populations using the subscripts 1 and 2 for convenience without loss of the generality.

IV. DYNAMICAL TRANSITIONS

In this section, we will proceed to unravel the dynamics and the phase transitions of the Sakaguchi-Kuramoto model (2) by constructing appropriate two parameter phase diagrams.

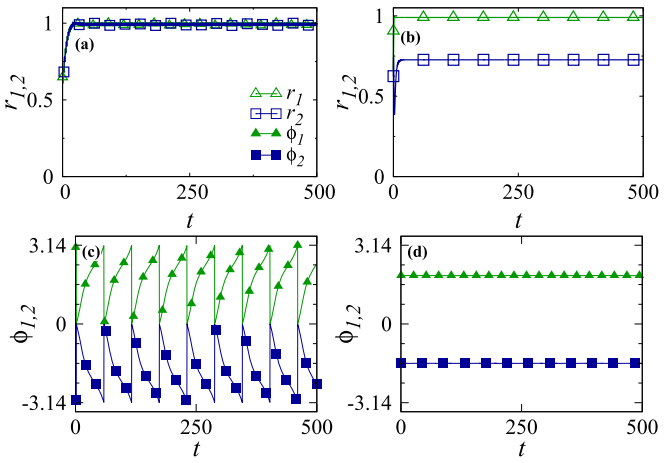

FIG. 1. The coexistence of the reflection symmetry preserving and reflection symmetry breaking self-organizing collective dynamical states. (a) and (b) The order parameters $r_{1,2}(t)$ corresponding to the two populations depicting the coexisting synchronized state and the static chimera state, respectively. (c) and (d) The order parameters $\phi_{1,2}(t)$ depicting the reflection symmetry $[\phi_1(t) = -\phi_2(t)]$ preserving oscillatory nature of the synchronized state and the reflection symmetry broken $[\phi_1(t) \neq -\phi_2(t)]$ static chimera state, respectively. The values of the parameters are $\omega = 2$, $K = 0.7$, and $\alpha = 0.3$.

We also classify the underlying self-emerging collective dynamical states from the bifurcation and theoretical analysis of the evolution equations corresponding to the macroscopic order parameters. We also solve the associated Sakaguchi-Kuramoto model by numerically integrating Eq. (2) to verify the dynamical transitions observed in the phase diagrams. The number of oscillators in both populations is fixed as $N^\sigma = 10^3$. We use the standard fourth-order Runge-Kutta integration scheme with an integration step size 0.01 to solve the system (2). The initial state of the oscillators (θ_i) is distributed with random phases between $-\pi$ and $+\pi$.

The macroscopic order parameters $r(t)$ and $\phi(t)$, obtained by numerically solving Eq. (2), are depicted in Figs. 1 and 2 for two different coupling strengths $K = 0.7$ and 1.5, respectively. The other parameters are fixed as $\omega = 2, \alpha = 0.3$.

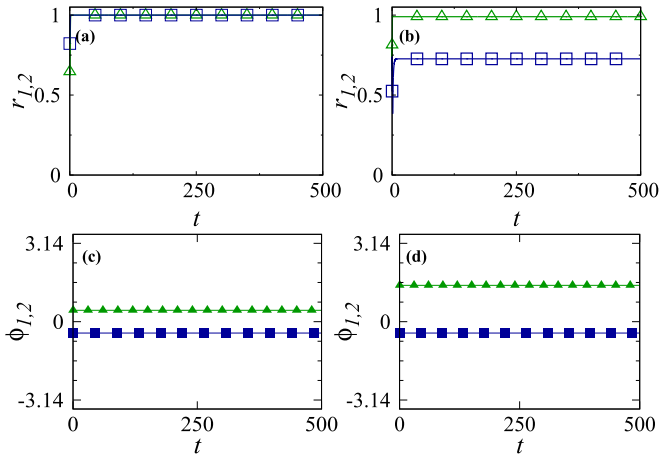

FIG. 2. Same as Fig. 1 for the coupling strength $K = 1.5$. Here, the synchronized state is a stable steady state.

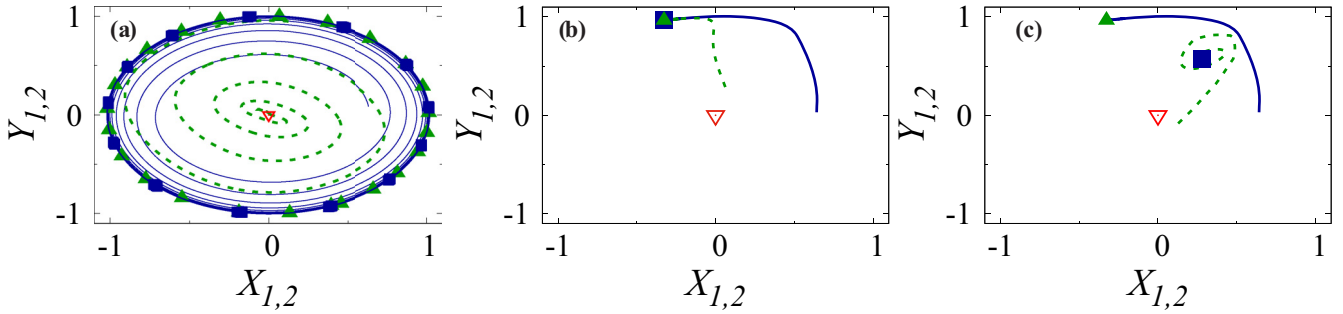

FIG. 3. Phase space dynamics of (a) the oscillatory synchronized state for $K = 0.4$, (b) the static synchronized state for $K = 2.0$, and (c) the static chimera state for $K = 2.0$. The unfilled inverted triangle corresponds to the unstable origin. The dashed and solid lines are the trajectories from two different initial conditions. Lines connected by filled triangles and squares correspond to the attractors of the first and second populations, respectively. The value of the other parameters are the same as in Fig. 1.

Left and right columns of Figs. 1 and 2 are depicted for two different initial conditions illustrating the two distinct coexisting self-organized dynamical states. The unit value of the order parameters $r_1(t)$ and $r_2(t)$ corresponding to the first and the second populations, respectively, in Fig. 1(a) corroborates the completely synchronized populations. However, one can also observe $r_1(t) = 1$ and $r_2(t) = 0.7$ [see Fig. 1(b)] for a different set of initial conditions characterizing that the first population evolve in synchrony, whereas the second population in partially synchrony elucidating the manifestation of the static chimera state. The reported chimera is associated with stationary chimera in the extensive world of chimeras as discussed in Ref. [42]. It is to be noted that the reflection symmetry $\phi_1(t) = -\phi_2(t)$ is preserved by the completely synchronized state [see Fig. 1(c)]. However, the static chimera state is manifested by breaking the reflection symmetry characterized by $\phi_1(t) \neq -\phi_2(t)$, where $\phi_1(t) = 1.93$ and $\phi_2(t) = -1.57$. Furthermore, the order parameters $\phi_{1,2}(t)$ in Fig. 1(c) reveal the oscillatory nature of the dynamical (synchronized) state.

The unit value of the order parameters $r_{1,2}(t)$ in Fig. 2(a) elucidates the synchronized state for $K = 1.5$. Note that the synchronized state is a reflection symmetry preserving static synchronized state as corroborated by the order parameters $\phi_{1,2}(t)$ depicted in Fig. 2(c). The order parameters corresponding to the coexisting partially synchronized state [see Fig. 2(b)] breaks the reflection symmetry [see Fig. 2(d)]. The corresponding attractors are depicted in the phase space $[X_{1,2} = r_{1,2}\cos(\phi_{1,2}), Y_{1,2} = r_{1,2}\sin(\phi_{1,2})]$ in Fig. 3. The unfilled inverted triangle corresponds to the unstable origin. The dashed and solid lines are the trajectories from two distinct initial conditions. The phase space of the oscillatory synchronized state is depicted in Fig. 3(a) for $K = 0.4$. The lines connected by filled triangles and filled squares correspond to the attractors of the first (always represented by triangles) and second (always represented by squares) populations, respectively, elucidating their oscillatory nature. The attractors, indicated by a filled triangle and a filled square, corresponding to the static synchronized state are depicted Fig. 3(b) for $K = 2.0$, whereas the attractors, indicated by a filled triangle (synchronized population) and a filled square (partially synchronized population), are depicted Fig. 3(c) for $K = 2.0$. The value of the other parameters are the same as in Fig. 1.

One parameter bifurcation diagrams obtained from the bifurcation analysis of the evolution equation for the complex mean-field variable z using the XPPAUT are depicted in the first row of Fig. 4 for three different values of the asymmetry parameter. The dotted lines correspond to the unstable steady states. The lines connected by filled circles correspond to the symmetry preserving synchronized OS state, which loses its stability via the homoclinic bifurcation at $K_{\mathrm{Hc}} = 1.82$ [see Fig. 4(a) for $\alpha = 0.1$] resulting in the symmetry preserving static synchronized state, indicated by dashed (blue) and solid (red) lines in the forward trace. Note that both populations remain synchronized in the explored range of K in the forward trace. However, in the reverse trace, the first population self-organizes to a static synchronized state, lines connected by filled triangles, in the range of $K \in [2, K_{\mathrm{SN}}]$ whereas the second population undergoes a transition from the reflection symmetry breaking (static steady) state, lines connected by filled squares, to the reflection symmetry preserving (synchronized oscillatory) state via the saddle-node (SN) bifurcation at $K_{\mathrm{SN}} = 1.64$. Only the symmetry preserving synchronized oscillatory state is observed in both populations in the range of $K \in [K_{\mathrm{SN}}, 1]$. In the region between K_{SN} and K_{Hc}, indicated by M1 both populations exhibit the synchronized oscillatory state in the forward trace. Nevertheless, the second population exhibits the symmetry breaking static steady state in the reverse trace whereas the first population is entrained to the synchronized steady state thereby elucidating the emergence of the static chimera state in both M1 and M2 regions. Hence, there is a bistability between the OS state and the static chimera state in the M1 region. For $K > K_{\mathrm{Hc}}$, the synchronized steady states of both populations coexist with the static chimera state in the M2 region. It is to be noted that the chimera state is observed even for a very low value of the asymmetry parameter α unlike the existing reports in the literature, where chimera states are observed only near $\pi/2$ values of the asymmetry parameter. Furthermore, the symmetry breaking chimera state is observed in the employed two populations of globally coupled Sakaguchi-Kuramoto model [4] only with the identical intrapopulation and interpopulation coupling strengths. The nonidentical intrapopulation and interpopulation coupling strengths as in Ref. [16] results only in the symmetry preserving synchronized states as shown in the Appendix.

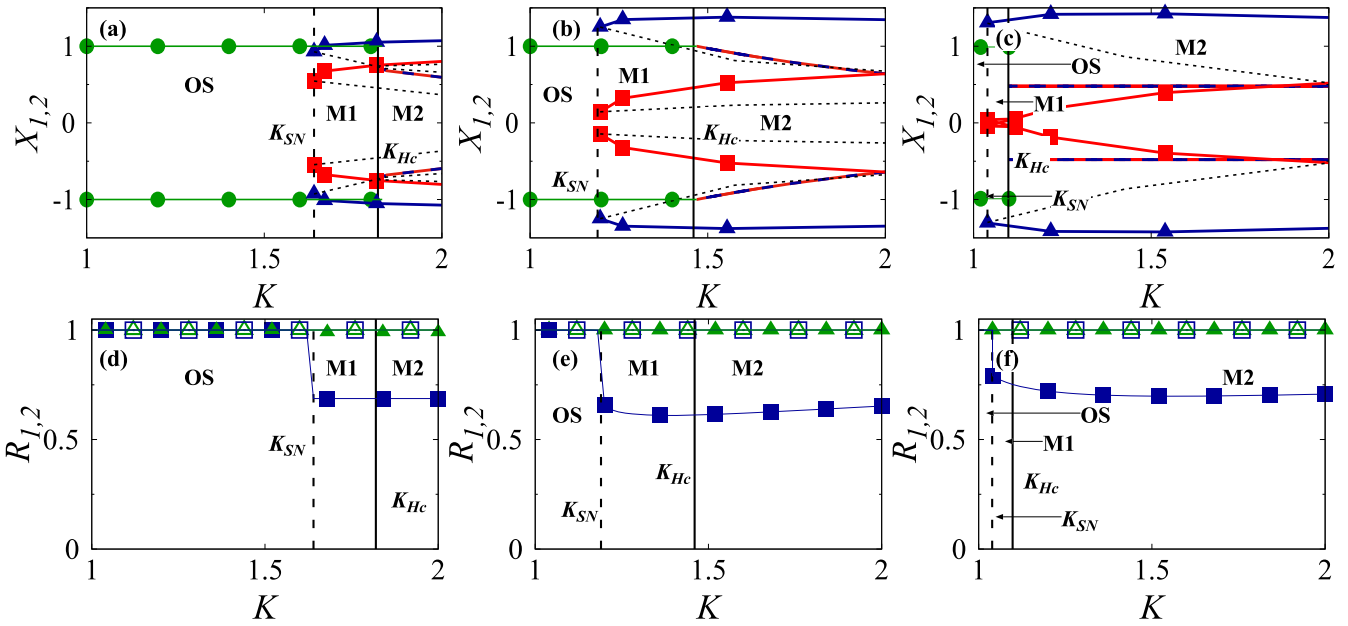

FIG. 4. One parameter bifurcation diagrams, obtained from the evolution equation for the mean-field variable $z = X + iY$ using XPPAUT, for the asymmetry parameter (a) $\alpha = 0.1$, (b) $\alpha = 0.3$, and (c) $\alpha = 1.0$ for $\omega = 2.0$. The corresponding time averaged order parameter R corroborating the dynamical transition is depicted in (d)–(f), respectively. Top row: The lines connected by filled circles correspond to the synchronized (OS) state, whereas the dashed (blue) and solid (red) lines for $K > K_{\rm Hc}$ correspond to the synchronized steady state in the forward trace. Dotted lines correspond to the unstable steady states. The lines connected by the filled triangles correspond to the synchronized steady state of the first population, whereas the lines connected by the filled squares correspond the symmetry breaking steady state of the second population in the reverse trace. Note that there is a transition from reflection symmetry breaking steady state to the symmetry preserving synchronized oscillatory state of the second population at $K = K_{SN}$. Bottom row: Forward trace is represented by lines connected by unfilled symbols, whereas the reverse trace is represented by lines connected by filled symbols. The lines connected by triangles illustrate the dynamical transitions of the first population, whereas the lines connected by squares elucidate the dynamical transitions of the second population. Note that there is an abrupt transition from the symmetry breaking state to the symmetry preserving state in the entire explored range of the asymmetry parameter. Solid and dashed vertical lines are the analytical critical curves corresponding to the homoclinic and saddle-node bifurcations, respectively. M1 and M2 are the bistable regions.

The vertical solid line at $K_{\rm Hc}$ is the homoclinic bifurcation curve across which the synchronized oscillatory state is manifested as the synchronized steady state. As the latter is characterized by $r_1 = r_2 = r = 1$ and $\phi_1 = -\phi_2 = \phi$, the condition for the homoclinic curve can be deduced as follows. Equation (6a) can be expressed in evolution equation in r and ϕ as

$$\dot{r} = \frac{K}{2}(1 - r^2)r[\cos(2\phi + \alpha) + \cos(\alpha)], \tag{7a}$$

$$\dot{\phi} = \omega - \frac{K}{2}(r^2 + 1)[\sin(2\phi + \alpha) - \sin(\alpha)]. \tag{7b}$$

Equating the left hand side of the above equations to zero, as it corresponds to the evolution equation for the synchronized steady state, and using $r = 1$, ϕ can be determined as $\phi = \frac{1}{2}\arcsin(\frac{\omega + K\sin(\alpha)}{K} - \alpha)$. By linearizing Eq. (7) about r and ϕ, the corresponding Jacobian matrix can be obtained as

$$J = \begin{bmatrix} K[\cot\left(\frac{\omega + K\sin(\alpha)}{K}\right) - \cos(\alpha)] & 0 \\ -\omega & -2K\cot\left(\frac{\omega + K\sin(\alpha)}{K}\right) \end{bmatrix}. \tag{8}$$

The eigenvalues of the above Jacobian matrix are expressed as

$$\lambda_1 = -2K\sqrt{1 - \frac{[\omega + K\sin(\alpha)]^2}{K^2}}, \tag{9a}$$

$$\lambda_2 = K\left(\sqrt{1 - \frac{[\omega + K\sin(\alpha)]^2}{K^2}} - \cos(\alpha)\right). \tag{9b}$$

The stability conditions for the homoclinic bifurcation curve are determined from the eigenvalues $\lambda_{1,2}$ as

$$K_{\rm Hc} = \frac{\omega}{1 + \sin(\alpha)}. \tag{10}$$

The analytic homoclinic bifurcation curve is depicted in Fig. 4 as the vertical solid line at $K = K_{\rm Hc}$, which matches exactly with the one parameter bifurcation diagram obtained from the XPPAUT. The static symmetry breaking steady state of the second population undergoes an abrupt bifurcation transition to the symmetry-preserving synchronized oscillatory state in the reverse trace at $K = K_{\rm SN}$. In the chimera state, the order parameter for the first population remains to be $r_1 = 1$, so the four coupled ordinary differential equations (ODEs) can be reduced to three coupled ODEs in $r_2 = r, \phi_1$, and ϕ_2.

Furthermore, it can also be reduced to two ODEs using $\nu=\phi_1-\phi_2$, whose evolution equations can be represented as

$$\dot{r} = \frac{K}{2}(1-r^2)[\cos(\nu+\alpha)+r\cos(\alpha)], \tag{11a}$$

$$\dot{\nu} = 2\omega + K\left[\frac{(r^2+1)}{2r}[\sin(\nu+\alpha)+r\sin(\alpha)] + \sin(\alpha)+r\sin(\nu+\alpha)\right]. \tag{11b}$$

Since the chimera state comprises of steady states of both populations, equating the left hand side of Eqs. (11) to zero, one can obtain

$$r = \sec(\alpha)\cos(\nu+\alpha), \tag{12a}$$

$$\nu = \sin^{-1}\left(\frac{4r\omega}{K(1+3r^2)} + \frac{r(3+r^2)\sin(\alpha)}{1+3r^2}\right) - \alpha. \tag{12b}$$

Linearizing Eqs. (11) about r and ν will result in the stability condition for the saddle-node bifurcation. Equating the determinant of the corresponding Jacobian to zero, one can obtain

$$\frac{K}{4}\left(2r^2(1+3r^2)\cos^2(\nu+\alpha)+(r^2-1)(2r^3\sin(\alpha) + (3r^2-1)\sin(\nu+\alpha))\sin(\nu+\alpha) - r(9r^4-1)\cos(\alpha)\cos(\nu+\alpha)\right) = 0. \tag{13}$$

Substituting r and ν in the above equation results in the saddle-node bifurcation condition represented as

$$A^2\cos(\alpha)+(2(A^2+8\omega^2)+24A\omega\sin(\alpha)+9A^2\sin(\alpha)^2)Q_1+6A^2\cos(\alpha)Q_1^2+6(16\omega(\omega+24A\sin(\alpha)) + 3A^2(3\sin(\alpha)^2-1))Q_1^3+2(8(A^2-3\omega^2)+19A^2\cos(2\alpha)-68A\omega\sin(\alpha))Q_1^5+54A^2\cos(\alpha)Q_1^6+A^2(49+5\cos(2\alpha))Q_1^7 - 81(A^2)\cos(\alpha)Q_1^8+3A^2\sin(\alpha)^2Q_1^9=0, \tag{14}$$

where $A=K/4$, and

$$Q_1 = \csc(\alpha)+32^{2/3}[A^3\cos(\alpha)^2]\csc(\alpha) + \frac{1}{2^{2/3}}\{3A\csc(\alpha)[3A+3A\cos(2\alpha)-8\omega\sin(\alpha)]\}.$$

The parameters satisfying Eq. (14) leads to the stability condition for the saddle-node bifurcation, depicted as the vertical dashed line in Fig. 4 at $K=K_{\mathrm{SN}}$.

The time averaged order parameter R defined as

$$R = \lim_{t\to\infty}\frac{1}{\tau}\int_t^{t+\tau} r(t)dt, \tag{15}$$

is depicted as a function of the coupling strength K in the second row of Fig. 4 corresponding to the one parameter bifurcation diagrams in the first row of Fig. 4. The desynchronized state is characterized by $R=0$, whereas the synchronized state is characterized by $R=1$. The intermediate values of R between 0 and 1 correspond to the partially synchronized states. The lines connected by open symbols correspond to the forward trace, whereas the lines connected by filled symbols correspond to the backward trace. Lines connected by triangles characterize the dynamical transitions of the first population, whereas the lines connected by squares corroborate the dynamical transitions of the second population. The vertical dashed line (saddle-node bifurcation curve) at K_{SN} separates the monostable synchronized oscillatory state and the bistable region M1. Note that it essentially demarcates the reflection symmetry preserving state and the reflection symmetry breaking state. Similarly, the vertical solid line (homoclinic bifurcation curve) at K_{Hc} demarcates the bistable M1 region from the region of bistability between the symmetry preserving static synchronized state and the symmetry breaking chimera state, denoted as M2.

The nature of the dynamical transition as indicated by the time averaged order parameter R in the range of the coupling strength $K\in[1,2]$ for the asymmetry parameter $\alpha=0.1$ is depicted in Fig. 4(d). Note that both subpopulations remain in the synchronized state as corroborated by $R=1$, lines connected by unfilled symbols, in the forward trace. In contrast, there is an abrupt transition in the dynamics of the second population, line connected by filled squares, from the reflection symmetry broken static steady state to the reflection symmetry preserving synchronized oscillatory state in the reverse trace. The first population, line connected by filled triangles, remains in the synchronized state in the reverse trace as characterized by $R=1$. The time averaged order parameter R in Fig. 4(d) corroborates the bifurcation transitions observed in the corresponding one parameter bifurcation diagram in Fig. 4(a). Similar dynamical transitions are also observed in the one parameter bifurcation diagrams in Figs. 4(b) and 4(c) and the corresponding time averaged order parameter R in Figs. 4(e) and 4(f) for the asymmetry parameter $\alpha=0.3$ and 1, respectively. However, note that the bistable regions M1 and M2 are enlarged for $\alpha=0.3$ by a decrease in the OS region, whereas the bistable region M2 prevails almost in the entire range of $K\in(1,2)$ for $\alpha=1.0$ [see Figs. 4(c) and 4(f)]. The abrupt transition from the symmetry breaking state to the symmetry preserving state in the reverse trace is observed in the entire explored range of the asymmetry parameter.

Two parameter phase diagrams are depicted on the (K,ω) plane in Figs. 5(a) and 5(b) for $\alpha=0.3$ and 1, respectively. The synchronized oscillatory state, represented by diagonal lines, manifests as the synchronized steady state, represented by the checked region, across the analytic homoclinic bifurcation curve K_{Hc}, indicated by the solid line, during the forward trace as a function of K. Recall that both populations are completely synchronized during the forward trace. The first population transits from synchronized steady state, indicated by gray shaded region, to synchronized oscillatory state via the saddle-node bifurcation curve, indicated by the dashed

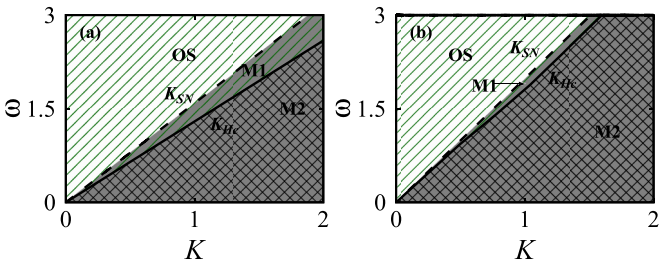

FIG. 5. Two phase diagram on the (K, ω) plane for the asymmetry parameter (a) α=0.3 and (b) $\alpha = 1$. The diagonal lines represent the symmetry preserving synchronized oscillatory state, the gray shaded region represents the symmetry breaking chimera state and the checked region represent the symmetry preserving synchronized steady state. The dashed and solid lines are the analytical critical curves corresponding to the saddle-node and homoclinic bifurcations, respectively.

line in the reverse trace. Furthermore, the second population exhibits a transition from the symmetry breaking steady state to the symmetry-preserving synchronized oscillatory state via the saddle-node bifurcation curve in the reverse trace. M1 and M2 are the bistable regions as discussed in the one parameter bifurcation diagrams. Increasing the asymmetry parameter increases the M2 region to an appreciable extent decreasing the M1 region and the region of the OS state [see Fig. 5(b) for $\alpha = 1$] in concurrence with the results observed in the one parameter bifurcation diagrams.

The phase diagram in the (α, K) space for $\omega = 2$ is depicted in Fig. 6. The intriguing collective dynamical states and the transition between them are similar to those observed in Fig. 5. It is clearly evident that the reflection symmetry breaking chimera state not just limited to near $\pi/2$ values of the asymmetry parameter as observed in existing literature [16–20,23,24,26,27], but, indeed, it extends to even near zero values of the asymmetry parameter for large coupling strengths thereby resulting in the manifestation of the chimera state in almost entire explored range of α. The shaded regions in Figs. 5 and 6 are obtained from the simulation of the original set of Eqs. (2), the boundaries of which are in excellent agreement with the analytical critical (bifurcation) curves.

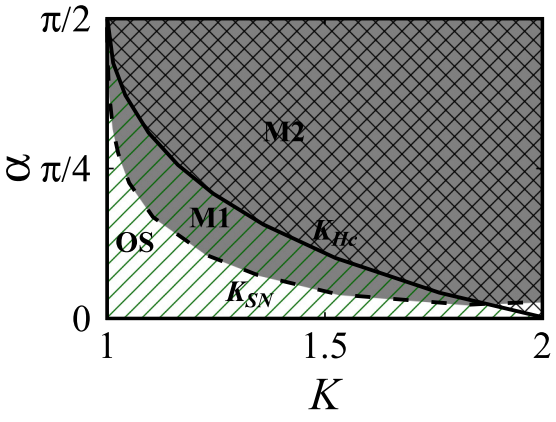

FIG. 6. Two phase diagram on the (K, α) plane for ω=2. The collective dynamical states and the bifurcation transitions are similar to those observed in Fig. 5.

V. CONCLUSIONS

We have considered two populations of globally coupled Sakaguchi-Kuramoto model with the same intra- and inter-population coupling strengths. The oscillators constituting the intrapopulation are chosen to be identical with the same frequency, whereas that constituting the interpopulations are chosen to have a parameter mismatch. The asymmetry parameters in the intra- and interpopulations are chosen such that there lies a permutation symmetry among the oscillators constituting intrapopulation and a reflection symmetry among the oscillators constituting the interpopulation. We have observed that the onset of the chimera state was accompanied by the manifestation of spontaneous breaking of the reflection symmetry among the inter-population unlike the existing literatures on two or more populations where the chimera states usually emerge by breaking the permutation symmetry among the interpopulation. Furthermore, we have also observed that the chimera state has manifested almost in the entire explored range of the asymmetry parameter, extending even to the near zero value of it, and the coupling strength in contrast to the existing literature where the onset of chimera states are restricted to near $\pi/2$ values of the asymmetry parameter and in a small range of the coupling strength. There is an abrupt transition of the second population from symmetry breaking steady state to the symmetry-preserving oscillatory synchronized state in the reverse trace via the saddle-node bifurcation. In the forward trace, both populations exhibit transition from the symmetry-preserving oscillatory synchronized state to symmetry preserving static synchronized state via the homoclinic bifurcation. We have also deduced the governing equations of motion for the macroscopic order parameters employing the finite-dimensional reduction by Watanabe and Strogatz [36]. The deduced analytical stability curves from the evolution equations of motion for the macroscopic order parameters corresponding to the saddle-node and homoclinic bifurcations are found to exactly match with the simulations results obtained from the original evolution equations of the globally coupled Sakaguchi-Kuramoto model and the bifurcation curves obtained using the software package XPPAUT. As the paradigmatic Kuramoto model can be reduced from the Stuart-Landau limit-cycle oscillator, which is the normal form of the supercritical Hopf bifurcation and, hence, the dynamics of any nonlinear oscillator exhibiting supercritical Hopf bifurcation can be described by the Stuart-Landau limit-cycle oscillator. This fact elucidates that the reported abrupt symmetry-preserving transition in the paradigmatic Kuramoto model is expected to be generic for a class of nonlinear oscillator exhibiting supercritical Hopf bifurcation.

ACKNOWLEDGMENTS

M.M. acknowledges the Department of Science and Technology, Government of India, for providing financial support through an INSPIRE Fellowship No. DST/INSPIRE Fellowship/2019/IF190871. The work of V.K.C. was supported by DST-CRG Project under

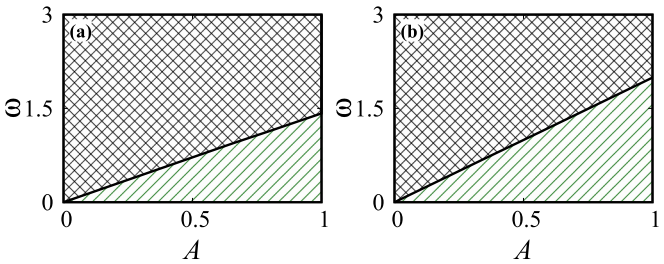

FIG. 7. The two phase diagram for the $(A-\omega)$ plane for asymmetry parameter, (a) α=0.8 and (b) α=1.5. Only the symmetry-preserving synchronized oscillatory state (indicated by diagonal lines) and steady state (indicated by checked region) is observed in the entire two parameter phase diagram.

Grant No. CRG/2020/004353, and V.K.C. wishes to thank DST, New Delhi for computational facilities under the DST-FIST programme (Grant No. SR/FST/PS-1/2020/135) to the Department of Physics. D.V.S. was supported by the DST-SERB-CRG Project under Grant No. CRG/2021/000816.

APPENDIX: SYMMETRY-PRESERVING STATES FOR NONIDENTICAL INTRAPOPULATION AND INTERPOPULATION COUPLING STRENGTHS

We have analyzed the two populations of globally coupled Sakaguchi-Kuramoto model [4] with intrapopulation coupling strength stronger than the interpopulation coupling strength as studied by Abrams *et al.* [16]. Accordingly, the coupling strengths in Eq. (2) will become $K^{11}=K^{22}=(1+A)$ and $K^{12}=K^{21}=(1-A)$, where $2A$ is the degree of mismatch in the intra- and interpopulation coupling strengths.

Two phase diagram in the $(\omega-A)$ parameter space is depicted in Figs. 7(a) and 7(b) for $\alpha=0.8$ and 1.5, respectively. It is to be noted that only the symmetry-preserving synchronized oscillatory, indicated by diagonal lines, and the steady state (indicated by the checked region) is observed in the entire parameter space in contrast to phase diagrams in the main paper and that in Abrams *et al.* [16]. Furthermore, increasing the asymmetry parameter α results in a large region of the oscillatory synchronized state [see Fig. 7(b)]. As the symmetry-preserving synchronized state is characterized by $r_1=r_2=r=1$ and $\phi_1=-\phi_2=\phi$, the condition for the homoclinic curve can be deduced as follows. Equation (6a) can be expressed in evolution equation in r and ϕ as

$$\dot{r}=(1-r^2)r\left(\frac{1+A}{2}\cos(\alpha)-\frac{1-A}{2}\cos(2\phi-\alpha)\right), \tag{A1a}$$

$$\dot{\phi}=\omega-(r^2+1)\left(\frac{1+A}{2}\sin(\alpha)+\frac{1-A}{2}\sin(2\phi-\alpha)\right). \tag{A1b}$$

By linearizing Eq. (A1) about r and ϕ, the eigenvalues of the corresponding Jacobian is obtained as

$$\lambda_1=\omega-2\,\sin(\alpha)-2A\,\sin(\alpha), \tag{A2}$$

$$\lambda_2=-(1+A)\cos(\alpha)+(A-1)\sqrt{1-\frac{\omega}{(1-A)}-\frac{((1+A)\sin(\alpha))}{(1-A)^2}}. \tag{A3}$$

The stability condition for the homoclinic bifurcation curve is determined from the above eigenvalues $\lambda_{1,2}$ as

$$A=\frac{1+\omega-\sin(\alpha)}{1-\sin(\alpha)}. \tag{A4}$$

The solid diagonal line in Fig. 7 corresponds to the homoclinic bifurcation curve $K_{\rm Hc}$ across which the synchronized oscillatory state is manifested as the synchronized steady state as ω is increased. Hence, it is evident that only identical intrapopulation and interpopulation coupling strengths in the employed two populations of globally coupled Sakaguchi-Kuramoto model [4] will results in the symmetry breaking chimera states as demonstrated in the main part of the paper.

[1] Y. Kuramoto and D. Battogtokh, Coexistence of coherence and incoherence in nonlocally coupled phase oscillators, Nonlinear Phenom. Complex Syst. **5**, 380 (2002).
[2] D. M. Abrams and S. H. Strogatz, Chimera States for Coupled Oscillators, Phys. Rev. Lett. **93**, 174102 (2004).
[3] Y. Kuramoto, Scaling Behavior of Turbulent Oscillators with Non-Local Interaction, Prog. Theor. Phys. **94**, 321 (1995).
[4] Y. Kuramoto and H. Nakao, Power-law spatial correlations and the onset of individual motions in self-oscillatory media with non-local coupling, Physica D **103**, 294 (1997).
[5] Y. Kuramoto, D. Battogtokh, and H. Nakao, Multiaffine Chemical Turbulence, Phys. Rev. Lett. **81**, 3543 (1998).
[6] Y. Kuramoto, H. Nakao, and D. Battogtokh, Multi-scaled turbulence in large populations of oscillators in a diffusive medium, Physica A **288**, 244 (2000).
[7] S. I. Shima and Y. Kuramoto, Rotating spiral waves with phase-randomized core in nonlocally coupled oscillators, Phys. Rev. E **69**, 036213 (2004).
[8] D. M. Abrams and S. H. Strogatz, Chimera states in a ring of nonlocally coupled oscillators, Int. J. Bifurcation Chaos **16**, 21 (2006).
[9] E. A. Martens, C. R. Laing, and S. H. Strogatz, Solvable Model of Spiral Wave Chimeras, Phys. Rev. Lett. **104**, 044101 (2010).
[10] M. R. Tinsley, S. Nkomo, K. Showalter, Chimera and phase-cluster states in populations of coupled chemical oscillators, Nat. Phys. **8**, 662 (2012).
[11] S. Nkomo, M. R. Tinsley, K. Showalter, Chimera States in Populations of Nonlocally Coupled Chemical Oscillators, Phys. Rev. Lett. **110**, 244102 (2013).
[12] L. V. Gambuzza, A. Buscarino, S. Chessari, L. Fortuna, R. Meucci and M. Frasca, Experimental investigation of chimera states with quiescent and synchronous domains in coupled electronic oscillators, Phys. Rev. E **90**, 032905 (2014).
[13] T. Banerjee, P. S. Dutta, A. Zakharova and E. Schöll, Chimera patterns induced by distance-dependent power-law coupling in ecological networks, Phys. Rev. E **94**, 032206 (2016).

[14] E. A. Martens, S. Thutupalli, A. Fourrière, and O. Hallatschek, Chimera states in mechanical oscillator networks, Proc. Natl. Acad. Sci. USA **110**, 10563 (2013).
[15] H. Yin, Chimera states in three populations of pendulum-like elements with inertia, American Journal of Physics and Applications **7**, 27 (2019).
[16] D. M. Abrams, R. Mirollo, S. H. Strogatz, and D. A. Wiley, Solvable Model for Chimera States of Coupled Oscillators, Phys. Rev. Lett. **101**, 084103 (2008).
[17] R. G. Andrzejak, G. Ruzzene and I. Malvestio, Generalized synchronization between chimera states, Chaos **27**, 053114 (2017).
[18] J. D. Hart, K. Bansal, T. E. Murphy and R. Roy, Experimental observation of chimera and cluster states in a minimal globally coupled network, Chaos **26**, 094801 (2016)
[19] M. G. Clerc, S. Coulibaly, M. A. Ferré, M. A. García-Ñustes, and R. G. Rojas, Chimera-type states induced by local coupling, Phys. Rev. E **93**, 052204 (2016).
[20] B. K. Bera, S. Majhi, D. Ghosh, and M. Perc, Chimera states: Effects of different coupling topologies, Europhys. Lett. **118**, 10001 (2017).
[21] A. Yeldesbay, A. Pikovsky, and M. Rosenblum, Chimeralike States in an Ensemble of Globally Coupled Oscillators, Phys. Rev. Lett. **112**, 144103 (2014).
[22] L. Schmidt and K. Krischer, Clustering as a Prerequisite for Chimera States in Globally Coupled Systems, Phys. Rev. Lett. **114**, 034101 (2015).
[23] V. A. Maksimenko, V. V. Makarov, B. K. Bera, D. Ghosh, S. K. Dana, M. V. Goremyko, N. S. Frolov, A. A. Koronovskii, and A. E. Hramov, Excitation and suppression of chimera states by multiplexing, Phys. Rev. E **94**, 052205 (2016).
[24] A. D. Kachhvah, and S. Jalan, Explosive synchronization and chimera in interpinned multilayer networks, Phys. Rev. E **104**, L042301 (2021)
[25] J. Sawicki, I. Omelchenko, A. Zakharova, and E. Schöll, Synchronization scenarios of chimeras in multiplex networks, Eur. Phys. J.: Spec. Top. **227**, 1161 (2018).
[26] E. V. Rybalova, A. Zakharova and G. I. Strelkova, Interplay between solitary states and chimeras in multiplex neural networks, Chaos, Solitons Fractals **148**, 111011 (2021).
[27] T. Kotwal, Xin Jiang, and D. M. Abrams, Connecting the Kuramoto Model and the Chimera State, Phys. Rev. Lett. **119**, 264101 (2017).
[28] S. Ghosh and S. Jalan, Emergence of chimera in multiplex network, Int. J. Bifurcation Chaos **26**, 1650120 (2016).
[29] R. Singh, S. N. Menon, and S. Sinha, Complex patterns arise through spontaneous symmetry breaking in dense homogeneous networks of neural oscillators Sci. Rep. **6**, 22074 (2016).
[30] A. Koseska, E. Volkov, J. Kurths, Transition from Amplitude to Oscillation Death via Turing Bifurcation, Phys. Rev. Lett. **111**, 024103 (2013).
[31] L. M. Pismen, Turing patterns and solitary structures under global control, J. Chem. Phys. **101**, 3135 (1994).
[32] I. Gowthaman, K. Sathiyadevi, V. K. Chandrasekar, and D. V. Senthilkumar, Symmetry breaking-induced state-dependent aging and chimera-like death state, Nonlinear Dyn. **101**, 53 (2020).
[33] V. K. Chandrasekar, R. Gopal, A. Venkatesan, and M. Lakshmanan, Mechanism for intensity-induced chimera states in globally coupled oscillators, Phys. Rev. E **90**, 062913 (2014).
[34] D. V. Senthilkumar and V. K. Chandrasekar, Local and global chimera states in a four-oscillator system, Phys. Rev. E **100**, 032211 (2019).
[35] U. Hananela, A. Ben-Moshea, H. Diamanta, and G. Markovich, Spontaneous and directed symmetry breaking in the formation of chiral nanocrystals, Proc. Natl. Acad. Sci. USA **116**, 11159 (2019).
[36] S. Watanabe and S. H. Strogatz, Constants of motion for superconducting Josephson arrays, Physica D **74**, 197 (1994).
[37] B. Ermentrout, *Simulating, Analyzing, and Animating Dynamical Systems: A Guide to XPPAUT for Researchers and Students*, (SIAM, Philadelphia, PA, 2002).
[38] A. Pikovsky and M. Rosenblum, Partially Integrable Dynamics of Hierarchical Populations of Coupled Oscillators, Phys. Rev. Lett. **101**, 264103 (2008).
[39] H. Hong and S. H. Strogatz, Conformists and contrarians in a Kuramoto model with identical natural frequencies, Phys. Rev. E **84**, 046202 (2011).
[40] E. Ott and T. M. Antonsen, Low dimensional behavior of large systems of globally coupled oscillators, Chaos **18**, 037113 (2008).
[41] E. Ott and T. M. Antonsen, Long time evolution of phase oscillator systems, Chaos **19**, 023117 (2009).
[42] F. P. Kemeth, S. W. Haugland, L. Schmidt, I. G. Kevrekidis and K. Krischer, A classification scheme for chimera states, Chaos **26**, 094815 (2016).